Physics and Chemistry of the Earth 93 (2016) 12–23

Contents lists available at ScienceDirect

Physics and Chemistry of the Earth

journal homepage: www.elsevier.com/locate/pce

Application of satellite products and hydrological modelling for flood early warning

Sifan A. Koriche [a, *], Tom H.M. Rientjes [b]

[a] School of Civil and Environmental Engineering, Jimma Institute of Technology, Jimma University, P.O. Box 142, Jimma, Oromia State, Ethiopia
[b] Department of Water Resources, Faculty of Geo-Information Science and Earth Observation, University of Twente, Hengelosestraat 99, 7514 AE Enschede, The Netherlands

ARTICLE INFO

Article history:
Received 24 March 2015
Received in revised form
28 October 2015
Accepted 7 March 2016
Available online 19 March 2016

Keywords:
Flood early warning
Flood index
Satellite remote sensing
Hydrological modelling

ABSTRACT

Floods have caused devastating impacts to the environment and society in Awash River Basin, Ethiopia. Since flooding events are frequent, this marks the need to develop tools for flood early warning. In this study, we propose a satellite based flood index to identify the runoff source areas that largely contribute to extreme runoff production and floods in the basin. Satellite based products used for development of the flood index are CMORPH (Climate Prediction Center MORPHing technique: 0.25° by 0.25°, daily) product for calculation of the Standard Precipitation Index (SPI) and a Shuttle Radar Topography Mission (SRTM) digital elevation model (DEM) for calculation of the Topographic Wetness Index (TWI). Other satellite products used in this study are for rainfall-runoff modelling to represent rainfall, potential evapotranspiration, vegetation cover and topography. Results of the study show that assessment of spatial and temporal rainfall variability by satellite products may well serve in flood early warning. Preliminary findings on effectiveness of the flood index developed in this study indicate that the index is well suited for flood early warning. The index combines SPI and TWI, and preliminary results illustrate the spatial distribution of likely runoff source areas that cause floods in flood prone areas.

1. Introduction

Disasters cause much damage and distress in less developed countries with limited financial resources. Engineering structures to mitigate on devastating effects by an extreme event are often not in place whereas tools for early warning are not well developed. According to reports from the World Meteorological Organization (2009), approximately 70% of all disasters occurring in the world relate to hydro-meteorological events. Poor disaster management practices, limited financial resources and high population pressure are some common characteristics of less developed countries and often cause that large numbers of people are affected in case of extreme meteo-hydrological events such as floods or droughts. In countries like Ethiopia, floodings may cause enormous impacts on the environment and society in urbanized and rural areas with high population density in agricultural production areas close to river channels. Besides the tragic loss of lives, impacts of floods include damages to property and the environment. In many parts of Ethiopia, flood events are reported frequently. Floods are attributed to rivers that overflow the riverbanks to inundate the adjacent flood plains. Large scale riverine flooding in Ethiopia is common and typically observed in the flat, lowland parts of the river basin systems due to large runoff volumes as caused by high runoff production in upstream, mountainous areas (see Taddese et al., 2006). A major river basin with frequent flooding events is the Awash River Basin with largest part located in the Rift Valley (Guinand, 1999; Achamyeleh, 2003; NASA Earth Observatory, 2003). Awash River Basin probably is the most developed area in Ethiopia with major economic value for Ethiopia. Due to its strategic location and availability of land and water resources, the basin has high potential for economic development. In the basin, two large sugarcane factories as well as many large and small-scale irrigation projects contribute to the nation's development (Taddese et al., 2006). While less extreme flood events in the basin support livelihood of the population through flood irrigation, extreme events cause much damage for which a flood early warning system is needed urgently to mitigate on effects and to reduce on impacts.

Needs for development of Early Warning Systems (EWS) started to arise in 1970s and 1980s when the prolonged droughts and

* Corresponding author.
E-mail address: numarsanifa@gmail.com (S.A. Koriche).

http://dx.doi.org/10.1016/j.pce.2016.03.007
1474-7065/

famines in the West African Sahel and in the Horn of Africa occurred. ESIG-ALERT (2004) reports that EWS has been developed to reduce societal risks and vulnerability, but also to support sustainable development. According to United Nations International Strategy for Disaster Redaction (UNISDR, 2009), an EWS is defined as:

> *"The set of capacities needed to generate and disseminate timely and meaningful warning information to enable individuals, communities and organizations threatened by a hazard to prepare and to act appropriately and in sufficient time to reduce the possibility of harm or loss."*

Currently various organizations across the world are involved in flood forecasting and early warning at national, continental and global scale. However, in Africa web-based information systems that serve for on-going transnational flood forecasting and early warning are limited in number (Table 1). In Ethiopia, in the Upper and Middle Awash River Basin, various initiatives address the problem of flooding (Abraha, 2006; Alemayehu, 2007). Some of the institutes in Ethiopia dealing with flood management, forecasting and early warning are Ministry of Water Resource and Energy (MoWE), Addis Ababa University (AAU), and National Meteorology Agency (NMA) of Ethiopia (Thiemig et al., 2011). Much effort on flood disasters in Ethiopia focus on strengthening rescue and relief arrangements during and after the events. Efforts to simulate runoff production and to predict flood behavior for flood early warning are limited. Poor gauging of rainfall and runoff in many Ethiopian river systems add to this aspect, besides that limited financial resources constrain efforts. Initiatives to develop a flood early warning such as e.g. for the Nile basin (World Bank, 2007) are not known. A well-known initiative for flood early warning in European river basins is the European Flood Alert System (EFAS).

In Ethiopia, the EFAS methodology has also been tested for Juba–Shabelle River Basin, which is adjacent to the Awash River Basin. The objective of the application was to develop a flood early warning system using various meteorological data sets produced by probabilistic weather forecasts and the LISFLOOD hydrological model (Thiemig et al., 2010). However, for reasons such as limited budget and lack of *in-situ* based gauge data, it proved that the procedure used by EFAS for Awash River Basin essentially was not possible. Therefore, an alternative method with different information sources must be developed.

The most important inputs to understand the hydrological processes that cause catchment runoff are hydro-meteorological observations. For early warning and to facilitate forecasting, hydro-meteorological data must be available in real time, or alternatively, must be forecast such as the European Centre for Medium-Range Weather Forecasts (ECMWF). Real time data can be provided from weather radars, satellites and or automatic gauging stations networks (Billa et al., 2006; Budhakooncharoen, 2004) whereas ECMWF and numerical weather prediction (NWP) data is available from large scale General Circulation Models (GCM). Burger et al. (2009); Thielen et al. (2009); Thiemig et al. (2011) and Alemseged and Rientjes (2015) show that NWP plays an important role in providing input for hydrological models for early warning.

For a better understanding of the main drivers that cause floods in Awash River Basin, it is very important to understand the catchment hydrological behavior and related runoff production processes that cause flood events. Hence, performing rainfall runoff and stream flow modelling is the first step. Rainfall runoff models are a simplified and conceptualized representation of the real world and serve as a tool to transform meteorological processes (i.e., rainfall and evapotranspiration) into the catchment runoff responses. There are various reasons for using rainfall runoff models. The main reason relates to the difficulty to measure the dynamics of hydrological processes that cause runoff production in space and time (Beven, 2012). Also measuring networks often all not well designed, with poor density and do not allow to represent processes in space and time domains that cause floodings. These aspects also often necessitates to use models. For this study the LISFLOOD model was selected which is a spatially distributed hydrological rainfall runoff model developed by the Joint Research Centre (JRC) of the European Commission for simulating hydrological processes that occur in catchments (De Roo et al., 2000). Most of the data sets used in this study are remote sensing products since Awash River Basin must be considered ungauged by the very low number or stream flow gauging stations as well as weather stations. Hence, satellite-derived products as inputs to a model for developing flood early warning system is advocated and tested in this study since adequate temporal and spatial coverage is provided. The use of satellite data may overcome constrains induced by poor data availability although satellite data requires bias correction before use (Habib et al., 2014; Haile et al., 2013).

The main objective of this study is to develop a flood early warning system for the upper and middle Awash River Basin by using satellite remote sensing products and hydrological modeling. Satellite data can be used in various ways to evaluate flood potential but also to predict a flood event in case of extreme rainfall in the basin. In this study we developed and propose the use of a spatially distributed flood index map to indicate runoff source areas for flood early warning. The flood index combines the Standard Precipitation Index and the Topographic Wetness Index. This study shows that a relation can be established between the topographic wetness and actual runoff production areas by extensive rainfall in the basin, and the actual locations where flood events have occurred.

2. Study area and data

2.1. Study area

The Awash River Basin is the fourth largest catchment (110,000 km^2) in Ethiopia and the seventh in terms of mean annual runoff (4.6 BM^3). The total length of the main course is some 1200 km and is the principal stream of an endorheic drainage basin covering parts of Oromia, Somali, Amara and Afar Regional States.

Table 1
Flood forecasting and early warning initiatives in Africa (after Thiemig et al., 2011).

Initiatives	Organizations/Institutes/Country
Flood forecasting initiative	WMO
Associated Program on Flood Management	WMO and GWP
Flood Risk and Response Management Information System	FAO-SWALIM
Early Warning and Humanitarian Emergency Information Centre	Republic of Sudan
SERVIR-Africa	NASA, RCMRD & CATHALAC
African Early Warning and Advisory Climate Services in Africa	ACMAD
Global Flood Alert System	Japanese Infrastructure Development Institute
Early Warning System for Flood Events	ITHACA

The geographical location of the basin is between latitudes of 7°25′N and 12°25′N and longitude of 38°13′E and 43°17′E (Taddese et al., 2006). The area considered for this study only covers the upstream and some middle part of the basin since stream flow time series for the further downstream catchment area is unavailable. The area of study covers about 31,483 km^2 (Fig. 1).

The basin area is characterized by the Ethiopian plateau and the Rift Valley that covers most of the Awash River Basin. The topography of the plateau is generally flat with elevations ranging from 2000 to 2500 m. The climate of the Awash River Basin is affected by the Inter-Tropical Convergence Zone (ITCZ). The seasonal rainfall distribution in the basin results from the annual migration of the ITCZ. Plateaus in the basin (>2500 m.a.s.l.) mostly receive 1400 to 1800 mm of rainfall per year. Whereas, mid-altitude (600–2500 m.a.s.l.) and lowlands regions (<600 m.a.s.l.) receive rainfall of 1000 to 1400 mm, and less than 200 mm per year, respectively. The rainfall distribution in the highland areas is bimodal with a short rainy season during March and April and the long rainy season from June to September. The mean annual temperatures range from 20.8 to 29.0 °C and the annual average wind speed is 1.2 ms^{-1}. The soil types found in the study area, according to FAO classification-1998, are pellic vertisol, vertic cambisol, chromic luvisols, luvic phaeozems and lithosols (Halcrow, 2006; MoWE, 2011).

Major parts of the Awash Valley are well developed with sugarcane factories and irrigation agriculture. Large scale sugarcane factories 'Wanji-Shoa'and 'Matahara' are located 15 km south of Adama city and 10 km southeast of Matahara town, respectively. Besides these factories, there are many irrigation projects, such as 'Tendaho', 'Kesem', and 'Awash Agro-Industry'. In the upper part of the basin, sugarcane is the dominant crop but citrus fruits, vegetables (mainly tomatoes), maize, groundnut, and cotton are also grown. In the lower part cotton is the dominant crop with over 90% of the irrigated area on large farm enterprises (Taddese et al., 2006).

2.2. Data sets

For this study, satellite remote sensing products and ground-based data sets are used. Most of the satellite data used is freely available online data (Table 2). *In-situ* data is collected during a two-week field campaign in September 2013. As part of the field visit, Awash Basin Authority (ABA), Ministry of Water and Energy (MoWE), National Meteorological Agency (NMA) and Water Works Design and Supervision Enterprise (WWDSE) offices are visited to collect secondary data that was available by previous studies on the flooding problems. Meteo-hydrological variables, soil and land cover data are collected during the field campaign.

2.2.1. Data from offices

For this study rainfall, humidity, sunshine duration, maximum and minimum temperature, and stream flow data from available

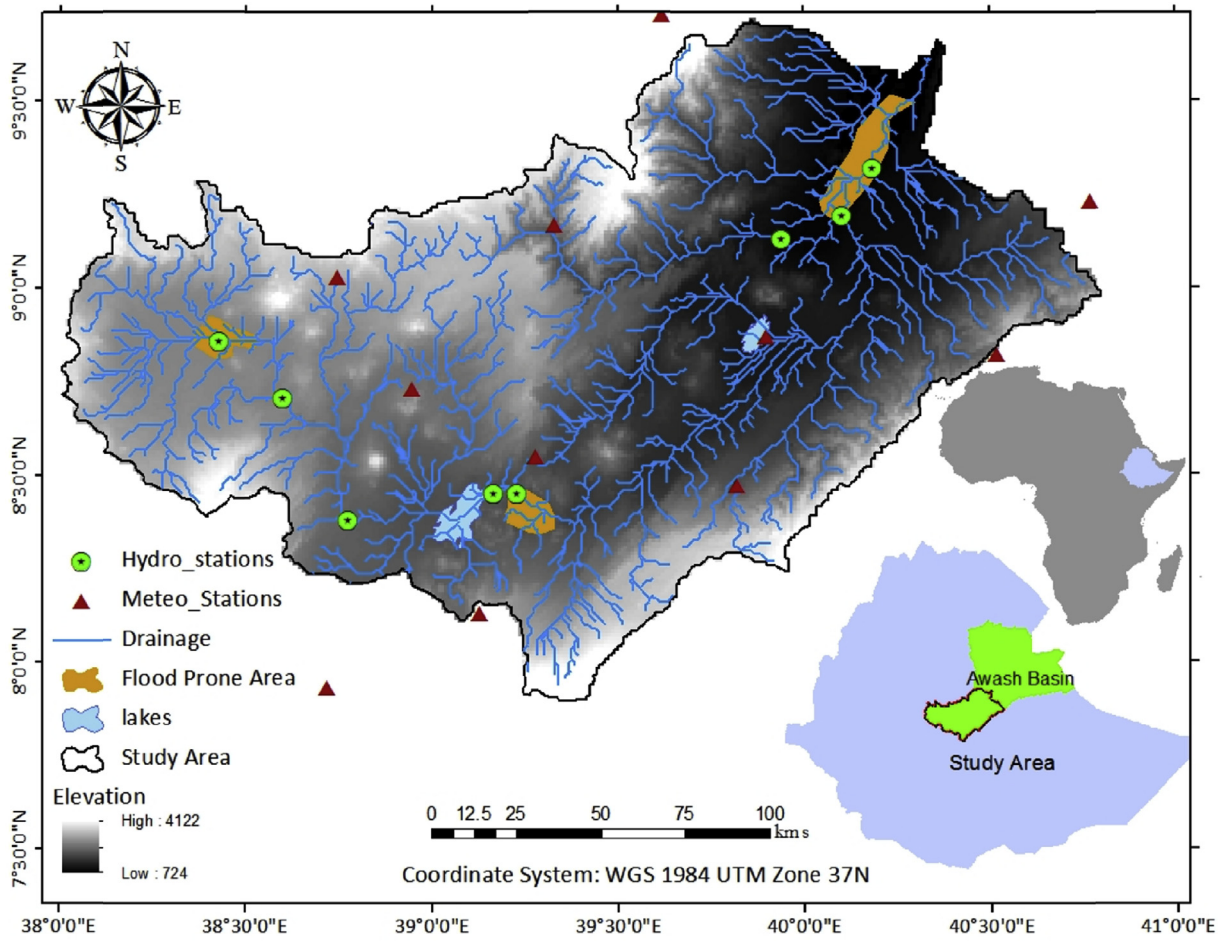

Fig. 1. Location map, topography, meteorological and hydrological stations of the study area (Data source: SRTM 90 m Digital Elevation Model and Ethiopian Ministry Water Resource).

Table 2
Satellite products with their spatial and temporal resolutions, source and period of records

Global CMORPH	Spatial resolution	0.25^0 by 0.25^0
	Temporal resolution	3hrs (accumulated to daily)
	Source (URL)	ftp://ftp.cpc.ncep.noaa.gov/precip/global_CMORPH/3-hourly_025deg
SAF Leaf Area Index (LAI)	Spatial resolution	3km
	Temporal resolution	Daily
	Source (URL)	http://landsaf.meteo.pt
FEWS NET Global Potential Evapotranspiration (PET)	Spatial resolution	1^0 by 1^0
	Temporal resolution	Daily
	Source (URL)	http://edcftp.cr.usgs.gov/pub/data/fewsips/global/
SRTM (DEM)	Spatial Resolution	1km
	Source (Jarvis et al., 2008)	http://srtm.csi.cgiar.org/SELECTION/inputCoord.asp

stations in the basin are collected. Also, a digital soil map based on FAO classification-1998 and land cover map produced from MODIS image is obtained from Awash Basin Authority (ABA). Stream flow time series from 6 river gauging stations that are located in the main river reach and in tributaries are obtained from MoWE. For 12 meteorological stations time series data is obtained from NMA (Fig. 1). Time series of the stream flow data are not always complete and are screened and corrected prior to modelling. The selection of suitable gauge(s) with reliable records for model calibration and validation was challenging, because of missing data and small gaps in the observed stream flow time series. Consistency of time series was examined by double mass curve analysis.

2.2.2. Satellite data products

Remote sensing products used for this study were CMORPH (precipitation), Satellite Application Facility-Leaf Area Index (LAI), FEWS NET Global Potential Evapotranspiration (PET) and SRTM-DEM (Jarvis et al., 2008). CMORPH (Climate Prediction Centre MORPHing technique) products are global precipitation products in which information from a number of independent data sources are merged. In Joyce et al. (2004) it is described that precipitation estimates are derived from the passive microwaves aboard the DMSP 13, 14 & 15 (SSM/I), the NOAA-15, 16, 17 & 18 (AMSU-B), and AMSR-E and TMI aboard NASA's Aqua and TRMM spacecraft, respectively. According to Liu et al., (2015) and Dinku et al., (2007) CMORPH shows better performing precipitation data at a daily time scale compared to TRMM in the Poyang Lake Basin of China and over east Africa respectively.

EUMETSAT promotes several Satellite Application Facilities (SAF's), among them the Land Surface Analysis-SAF which is dedicated to the development and operational retrieval of products from Meteosat Second Generation (MSG) and Meteorological Operational satellite program (MetOp) satellites over continental areas. Leaf area index (LAI) is one of the products estimated from the MSG SEVIRI instrument over Europe, Africa, the Middle East, and parts of South America and is available since January 2007. The product is available through the Land Surface Analysis-SAF web page. A detailed description of the processing algorithm and product description can be found on the product user manual available on EUMETSAT website (www.eumetsat.int/). LAI is an important input for hydrological modelling by means of LISFLOOD since it is used as input to simulate processes such as interception, evaporation of intercepted water, water uptake by plants roots and transpiration, and direct evaporation from the soil surface (Chen and Black, 1992; Roujean and Lacaze, 2002).

The daily global potential evapotranspiration (PET) is obtained from FEWS NET data portal. PET is one of the important forcing terms in hydrological modelling and in this study is calculated from climate parameter data of Global Data Assimilation System (GDAS) on a spatial basis using the Penman-Monteith equation (Allen et al., 1998, 2005; FEWS NET, 2011).

All satellite products except the SRTM-DEM can be processed using the GEONETCast toolbox plug-in under ILWIS (Maathuis et al., 2014). The temporal and spatial resolution and sources of the data sets used are indicated in Table 2.

3. Methodology

As a first step to flood early warning a rainfall runoff model based on the LISFLOOD model approach (Van der Knijff and De Roo, 2008) was developed. The LISFLOOD model has been selected for this study since it has applications in a number of catchments in Europe and the Horn of Africa (i.e., Juba-Shabelle basin in Somalia) for the purpose of flood forecasting and for development of a flood early warning system (De Roo et al., 2000; Thiemig et al., 2010). As indicator to basin wetness in this study, Topographic Wetness Index (TWI) and the Standardized Precipitation Index (SPI) are computed and combined in a spatially distributed flood index. The relation between locations with high flood index values and highest stream flow is established to serve flood early warning. The approach is depicted in Fig. 2 by means of a flow chart.

3.1. LISFLOOD model

Hydrological processes represented in LISFLOOD are snowmelt, infiltration, interception of rainfall, evaporation and water uptake by vegetation, surface runoff, preferential flow (bypass of soil layer), exchange of soil moisture between the two soil layers and drainage to the groundwater, sub-surface and groundwater flow and flow through river channels. LISFLOOD is driven by meteorological variables: precipitation, P ($mmday^{-1}$); potential (reference) evapotranspiration of a closed canopy, ET_0 ($mmday^{-1}$); potential evaporation from a bare soil surface, ES0 ($mmday^{-1}$); potential evaporation from open water, EW0 ($mmday^{-1}$); and average 24-h temperature, T_{avg} (°C). In the model, hydrological processes of a catchment are represented by a 2-layer soil water balance sub-model, and sub-models for groundwater and subsurface flow (using two parallel interconnected linear reservoirs), a sub-model for routing of surface runoff to the river channel and finally a sub-model for routing of stream flow in a channel (see Fig. 3). The above description is adapted from Van der Knijff and De Roo (2008), for a detailed description on processes, equations and assumptions reference is made to the same article.

De Roo et al. (2003) developed a distributed catchment model LISFLOOD for the Oder Basin (The Czech Republic, Poland and Germany) and the Meuse catchment (France, Belgium, Germany and The Netherlands) to investigate the cause of flooding and the influence of land use, soil characteristics and antecedent catchment moisture conditions. By using the model for the Meuse catchment, it was shown that land use changes between 1975 and 1992 have

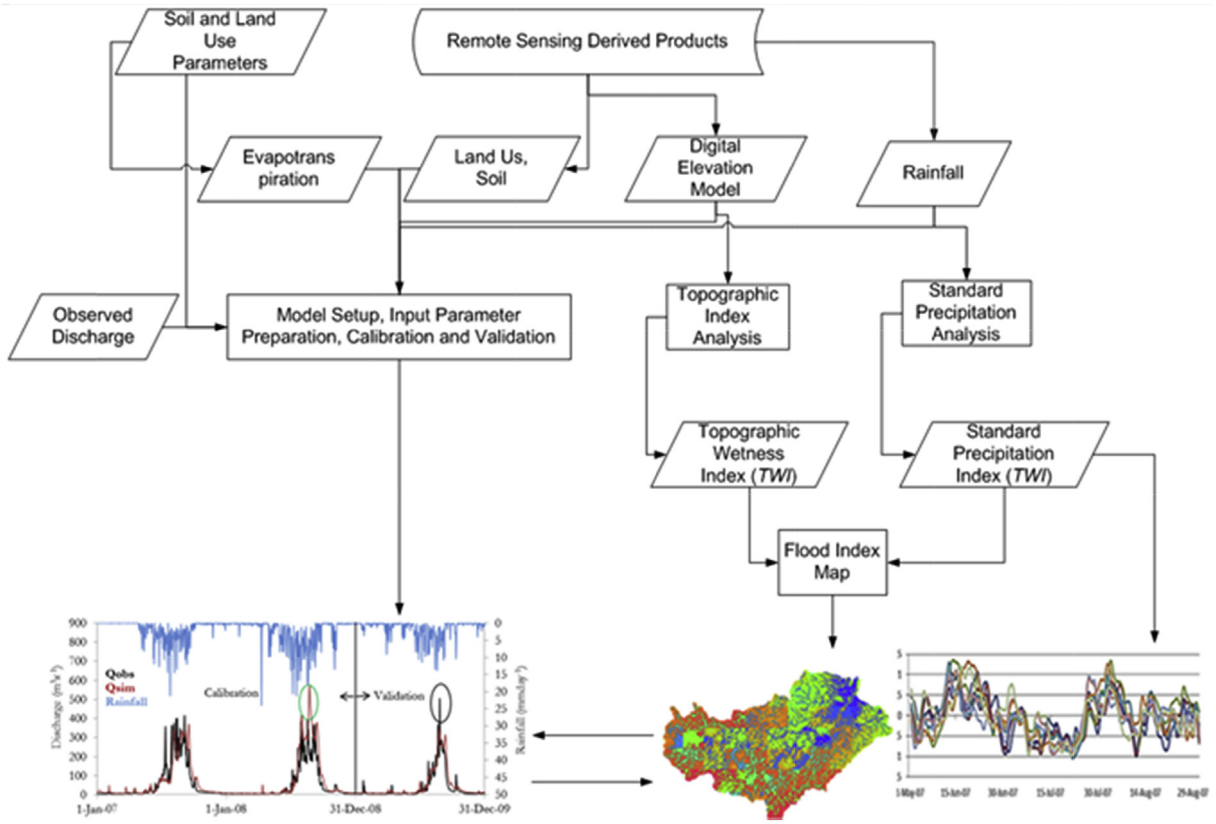

Fig. 2. Flowchart of the flood early warning approach. The figure shows two major step and or methods followed to achieve the objective of the research (to examine the relation between locations with high flood index values and highest stream flow: to serve in flood early warning). Runoff modelling (left panel) based on the LISFLOOD model approach and flood index (right panel) as indicator to basin wetness using TWI (from DEM) and SPI (CMORPH Rainfall).

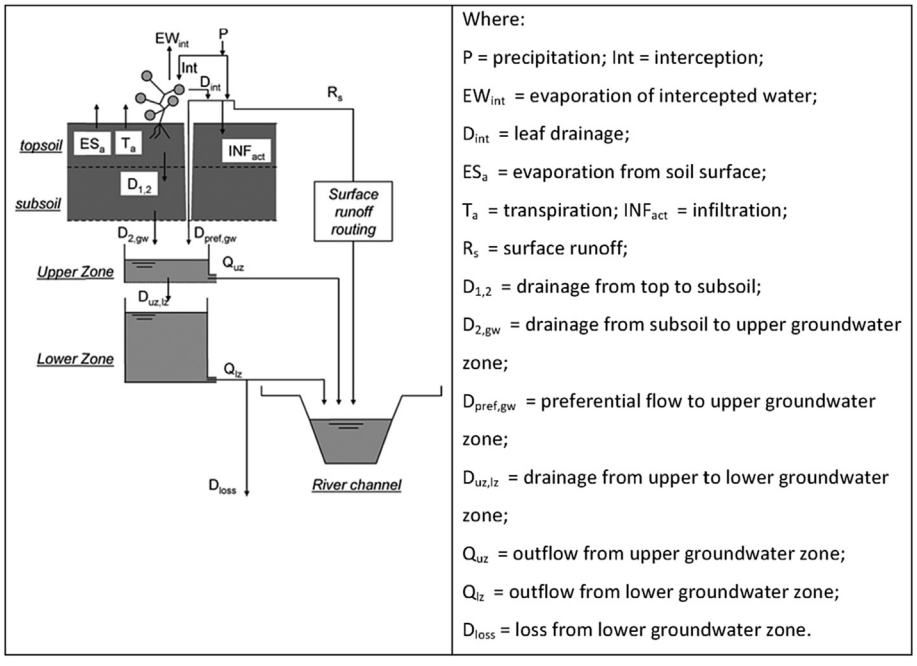

Fig. 3. Schematic representation of LISFLOOD model excluding snowmelt (Source: Van der Knijff and De Roo, 2008).

caused increased flood risks. Laguardia and Niemeyer (2008) compared the LISFLOOD estimated and satellite based ERS/SCAT soil moisture estimates over European catchments. Results indicated that LISFLOOD simulated and ERS/SCAT soil moisture products matched well over large areas in Europe, except for the Scandinavian regions. Dankers et al. (2007) used high-resolution

Table 3
Calibration parameters of the LISFLOOD model (Source: Feyen et al., 2007).

Parameters	Upper and lower limit	Description
Upper zone time constant (UZTC)	1–10	Control the amount and timing of outflow upper groundwater reservoirs
Lower zone time constant (LZTC)	10–5000	Control the amount and timing of outflow lower groundwater reservoirs
Ground water percolation value (GWPV)	0–0.5	Controls the flow from the upper to the lower groundwater zone
Xinanjiang parameter b (Xb)	0.05–0.5	controls the fraction of saturated area within a grid cell that is contributing to runoff
Power preferential bypass flow (PPBF)	5–15	Relates preferential flow with the relative saturation of the soil

climate model (HIRHAM) data to drive the hydrological model LISFLOOD for simulating flood hazards in the upper Danube basin (Europe). In the latter study, LISFLOOD has shown good model performance as long as the predictions from the climate model are representative. It was shown that accuracy of the climate model predictions affected accuracy of LISFLOOD. Salamon and Feyen (2009) have applied sequential data assimilation with the particle filter to assess effects of parameter uncertainty, precipitation uncertainty, and uncertainty of predictions of the LISFLOOD model for the Meuse catchment upstream of Borgharen (Maastricht, the Netherlands). Feyen et al. (2007) performed automated calibration using daily discharge observations from the Meuse catchment (France, Belgium, Germany and The Netherlands) to assess the model performance by applying the Shuffled Complex Evolution Metropolis (SCEM-UA) global optimization algorithm. Findings showed that the SCEM-UA algorithm was able to optimise most sensitive parameter values and to establish posterior parameter distributions in less than 2500 iterations using 2 years of daily stream flow data after Feyen et al. (2007).

LISFLOOD has shown acceptable performance in most studies it has been applied. Especially, the promising performance of the model in the tropical zone like Juba-Shabelle River Basin has contributed to the selection of the model for Awash River Basin. Furthermore, LISFLOOD is a physical based model, where the real world processes can be better represented compared to conceptual model, and most of the input data are freely available and spatially distributed.

3.2. Model calibration

For this study the Root Mean Square Error (RMSE) (Eq. (1)) and the Nash-Sutcliffe Coefficient of Efficiency (NSE) (Eq. (2)) and the Relative Volumetric Error (RV_e) (Eq. (3)) are selected as model performance indicators. The objective functions read:

$$RMSE = \sqrt{\frac{\sum_{i=1}^{n}\left(X_{obs,i} - X_{model,i}\right)^2}{n}} \quad (1)$$

$$RV_e = \left(\frac{\sum_{i=1}^{n} X_{model,i} - \sum_{i=1}^{n} X_{obs,i}}{\sum_{i=1}^{n} X_{obs,i}}\right) x\ 100 \quad (2)$$

$$NSE = 1 - \frac{\sum_{i=1}^{n}\left(X_{obs,i} - X_{model}\right)^2}{\sum_{i=1}^{n}\left(X_{obs,i} - X_{obs,mean}\right)^2} \quad (3)$$

Where: $X_{obs,i}$ are observed values, $X_{obs,mean}$ is the mean of the observation time series; and X_{model} are model estimated values, i stands for time instant. Both $RMSE$ and RV_e require minimisation, whereas NSE requires maximisation. When RV_e value is between −5% and +5% a good model performance is commonly assumed. NSE values higher than 0.8 suggest a good performance although interpreting values is not always trivial.

In LISFLOOD some parameter values can be set based on field measurements, whereas others require optimisation by model calibration. Van der Knijff and De Roo (2008) and Feyen et al. (2007) have shown that five parameters (Table 3) need to be estimated by calibration. In this study, a trial and error calibration was performed for the year 2007 and 2008. The optimised model parameter set is validated using daily stream flow time series for the year 2009.

3.3. SPI and TWI analysis as proxy to wetness distribution

To identify possible runoff source areas, this study aims to develop a spatially distributed flood index map by combining SPI and TWI. The flood index serves to indicate wetness and potential runoff production in basin by given rainfall event to serve flood early warning. SPI is an index which indicates the difference between observed precipitation and its mean value for a specified time period, which is divided by the standard deviation (McKee et al., 1993). Negative SPI values indicate dryness and positive indicates wetness as categorized in Table 4. The SPI is calculated using the following formula:

$$SPI = \frac{(X_i - X_{mean})}{\sigma} \quad (4)$$

Where: X_i is the accumulated daily (monthly) precipitation observation, X_{mean} is the mean daily (monthly) precipitation, and σ is the standard deviation.

The topographic wetness index is proposed in Beven and Kirkby (1979 and is developed to indicate the effect of local topography on upstream contributing areas. TWI indicates the tendency of water to accumulate at any point in the catchment and the downslope movement of water. A TWI map indicates the spatial distribution of wetness in a catchment with potential for surface saturation (modified after Beven and Kirkby, 1979). The topographic wetness index reads:

$$TWI = \ln\left(\frac{As}{\tan\beta}\right) \quad (5)$$

Where: As is the upslope contributing area per unit contour length; tanβ stands for the local slope in the steepest down slope direction of the terrain.

A map showing the distribution of TWI is a key element to geographically indicate the areas in a catchment with high potential to generate surface runoff. TWI has been used for a number of purposes, for example identification of subsurface flow sources,

Table 4
Category of SPI (adapted from McKee et al., 1993).

SPI Values	Categories
2.0 and above	Extremely wet
1.5 to 1.99	Very wet
1.0 to 1.49	Moderately wet
−0.99 to 0.99	Near normal
−1.0 to −1.49	Moderately dry
−1.5 to −1.99	Severely dry
−2.0 and less	Extremely dry

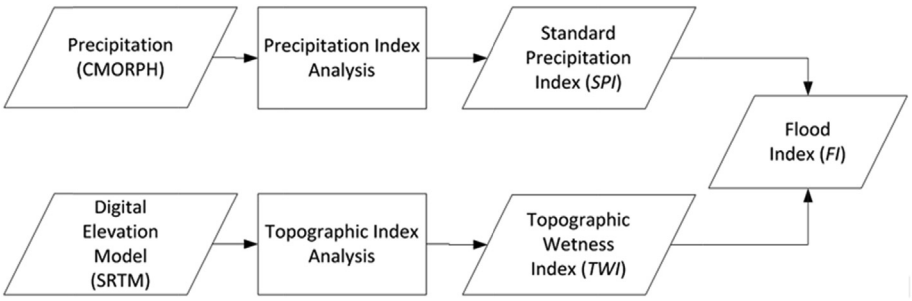

Fig. 4. Flowchart for combining SPI and TWI (Data source: CMORPH Rainfall Product and SRTM 90 m Digital Elevation Model).

assessment of hydrological, physical and chemical properties of soils or characterization of vegetation patterns (Moore et al., 1993; Robson et al., 1992; Seibert and McGlynn, 2007; Western et al., 1999).

The standard precipitation index (SPI) was developed for drought detection and monitoring. However, because of its characteristics, the SPI can also be used as a tool to detect and to indicate relatively wet conditions with above mean rainfall. The index may allow not only monitoring of meteo-hydrological conditions in a catchment, and more specific runoff source areas, but also the potential to warn for possible extreme events like a flood (after Seiler et al., 2002).

For mapping runoff source areas for flood early warning, in this study SPI and TWI maps were combined to create and generate a flood index map as shown in Fig. 4. Since in this study SPI map is updated on daily base by availability of satellite rainfall images at daily base, also a flood index map at daily base can be prepared. The flood index provides information on areas receiving above normal rainfall (attributed from SPI) and accounts for effects of local topography on the spatial distribution of runoff source area. TWI was calculated from a SRTM DEM of 1 km × 1 km resolution with values that ranged from 5 to 30 for the study area. Areas with high TWI (in this case ≥ 12.5) which are located in the vicinity of the main river were excluded so to only consider upstream runoff contributing areas for flood early warning.

Daily SPI maps were calculated from CMORPH rainfall product. The SPI maps of the wet period (June–August) for the years 2007, 2008 and 2009 were smoothed by applying a moving average window of 5 days to identify possible window(s) of time indicating high SPI values. Only positive SPI values were considered. Then, the values of both indices were normalized between 0 and 1. Finally, both indexes were combined after resampling to the same

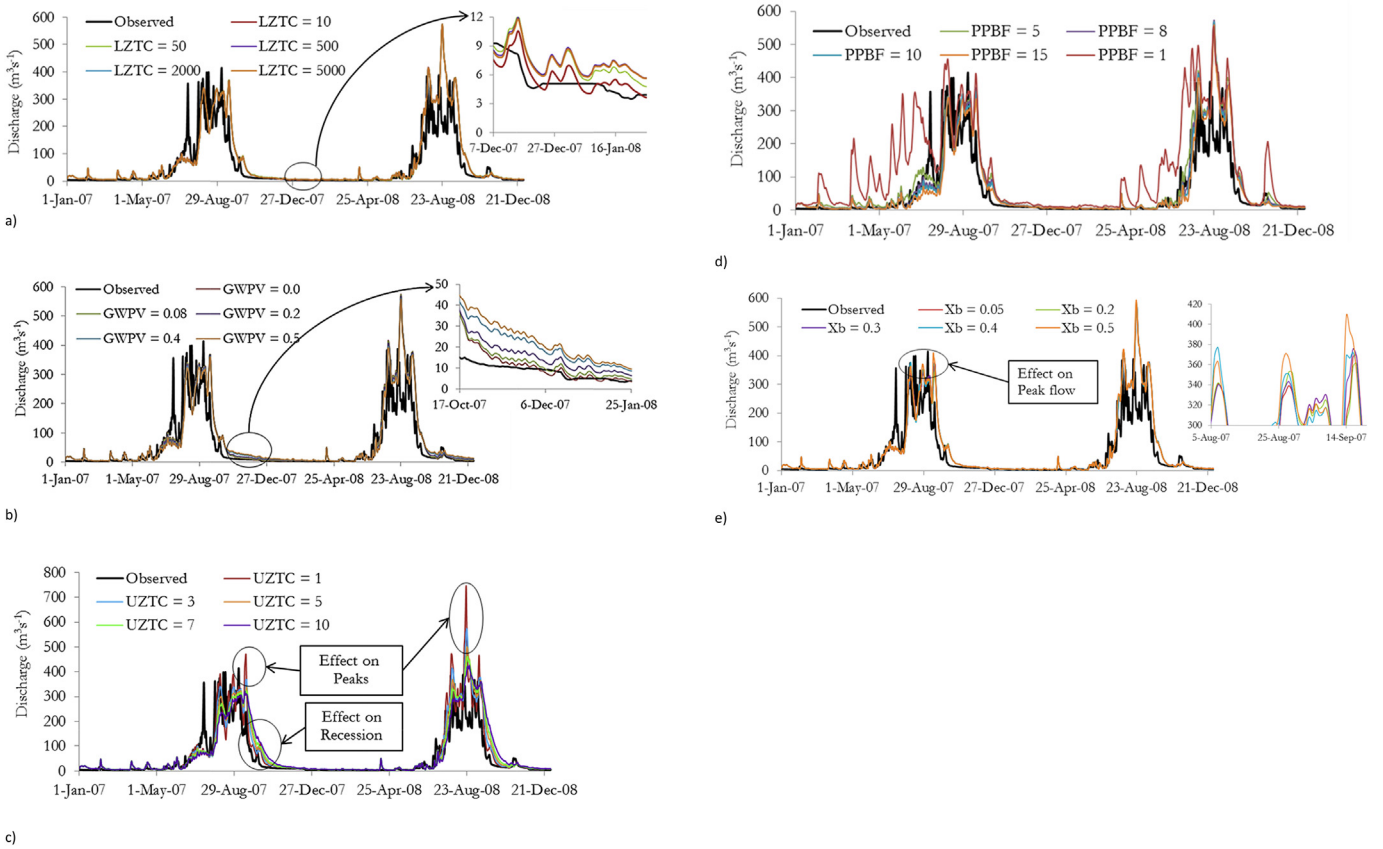

Fig. 5. Sensitivity of the LISFLOOD model to change in parameter value; a) Lower Zone Time Constant, b) GroundWater Percolation Value, c) Upper Zone Time Constant, d) Power Preferential Bypass Flow and e) Xinanjiang parameter.

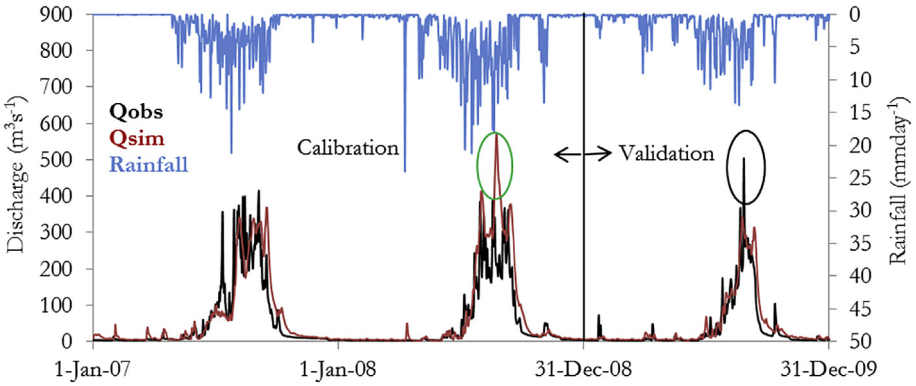

Fig. 6. Simulated (Qsim) and observed (Qobs) hydrograph for the period 2007–2009 at Melka Hombole gauge station (Data source: Observed Hydrograph from Ethiopian Ministry of Energy and Water Resource).

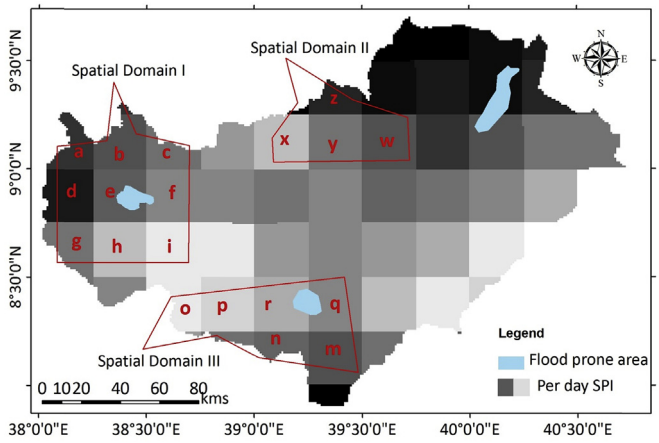

Fig. 7. Pixel locations were the SPI values of the wet season for the period June–August were taken. The respective letter symbol represent where the SPI pixel value was taken in the three spatial domains.

resolution (90 m) to produce a flood index map which changes in the time domain by SPI. Both SPI and TWI are assumed to equally affect the runoff production processes and thus equal weights were given. The following formula was used to combine both indexes to yield the combined index map.

$$FI = w1(TWI) + w2(SPI) \quad (6)$$

Where: FI = flood index; TWI = Topographic Wetness Index; SPI = Standard Precipitation Index; w1, w2 = weights.

In the study area three spatial domains have been selected to evaluate the temporal variation of the SPI, to examine the effect of upstream runoff contributing areas for flood early warning and to establish the relation between a flood index and highest stream flow (see Fig. 7).

4. Results and discussion

4.1. Calibration and validation results

Sensitivity of the five parameters (UZTC, LZTC, GWPV, Xb and PPBF) of the LISFLOOD model has been evaluated before performing calibration. Prior value ranges for the analysis and calibration are adapted from Feyen et al. (2007). The sensitivity analysis was done by changing one parameter at a time while the other parameters remained unchanged. For each of the parameters five different values were used to assess model sensitivity.

Results from the sensitivity analysis show that LZTC and GWPV affect the base flow part of the hydrograph. An increase in LZTC resulted in the decrease in the flow from the lower zone groundwater store as flux from the lower zone is inversely related to LZTC (see Fig. 5). An increase in GWPV resulted in an increase in base flow and a decrease in peak flows of the hydrograph, as the parameter controls the flow from the upper zone store to the lower zone groundwater store. When there is high percolation (high GWPV) from the upper zone groundwater store to the lower zone groundwater store, the amount of water available for quick flow decreases which leads to a decrease in peak flow discharges and the amount of low flow increases which leads to higher base flow. The other three parameters (UZTC, PPBF and Xb) affect quick flows from the upper zone. As the UZTC value increases the peak flow deceases and the slope of the falling limb of the hydrograph becomes less steep. This is because the parameter is formulated in such a way that it is inversely proportional to the discharge from the upper zone groundwater store. The PPBF value of 1 showed an unrealistic response of the catchment as the soil moisture store does not allow infiltration and any rainfall without delay transforms into stream flow from the model. Feyen et al. (2007) indicated that the PPBF value should not be less than 5.

A trial and error procedure was used to calibrate the model using the parameters in Table 3. In the calibration, qualitative and quantitative analyses have been performed. Based on comparison of observed and simulated stream flow hydrographs, adjustments

Table 5
Optimized parameter and objective functions' values for calibration and validation period

Optimized parameters values					**Objective functions**					
					Calibration			**Validation**		
UZTC [days]	LZTC [days]	GWPV [mmday^{-1}]	Xb [-]	PPBF [-]	RMSE [m^{3}s^{-1}]	NSE [-]	RVe [%]	RMSE [m^{3}s^{-1}]	NSE [-]	RVe [%]
3	10 - 500	0.08	0.05	8	55.29	0.72	0.27	29.37	0.82	21.07

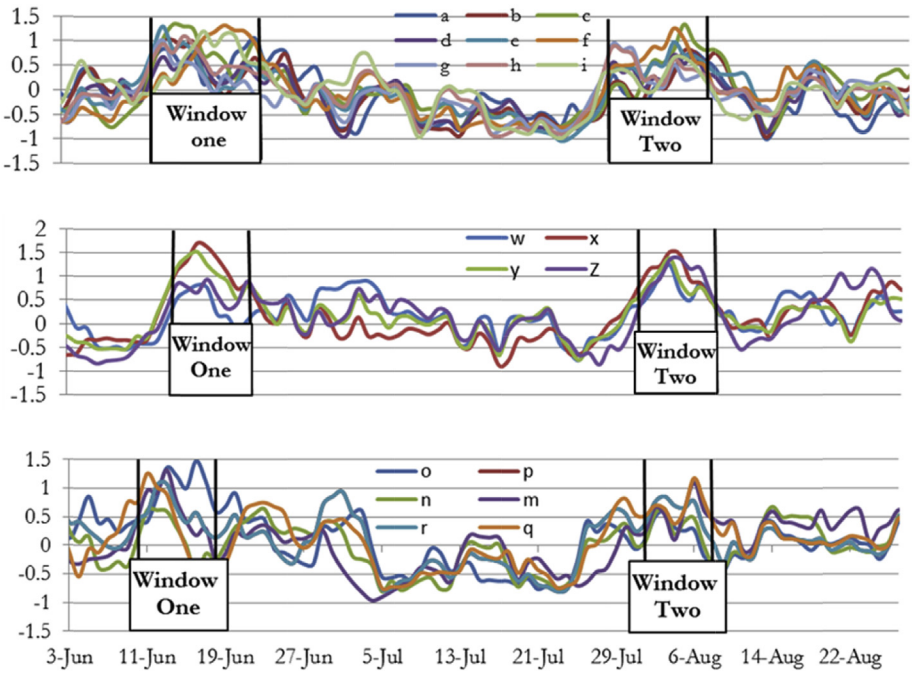

Fig. 8. Temporal variation of wet season SPI of the spatial domain I, II and III (see Fig. 7). The respective letter symbol represent where the SPI pixel value was taken in the three spatial domains.

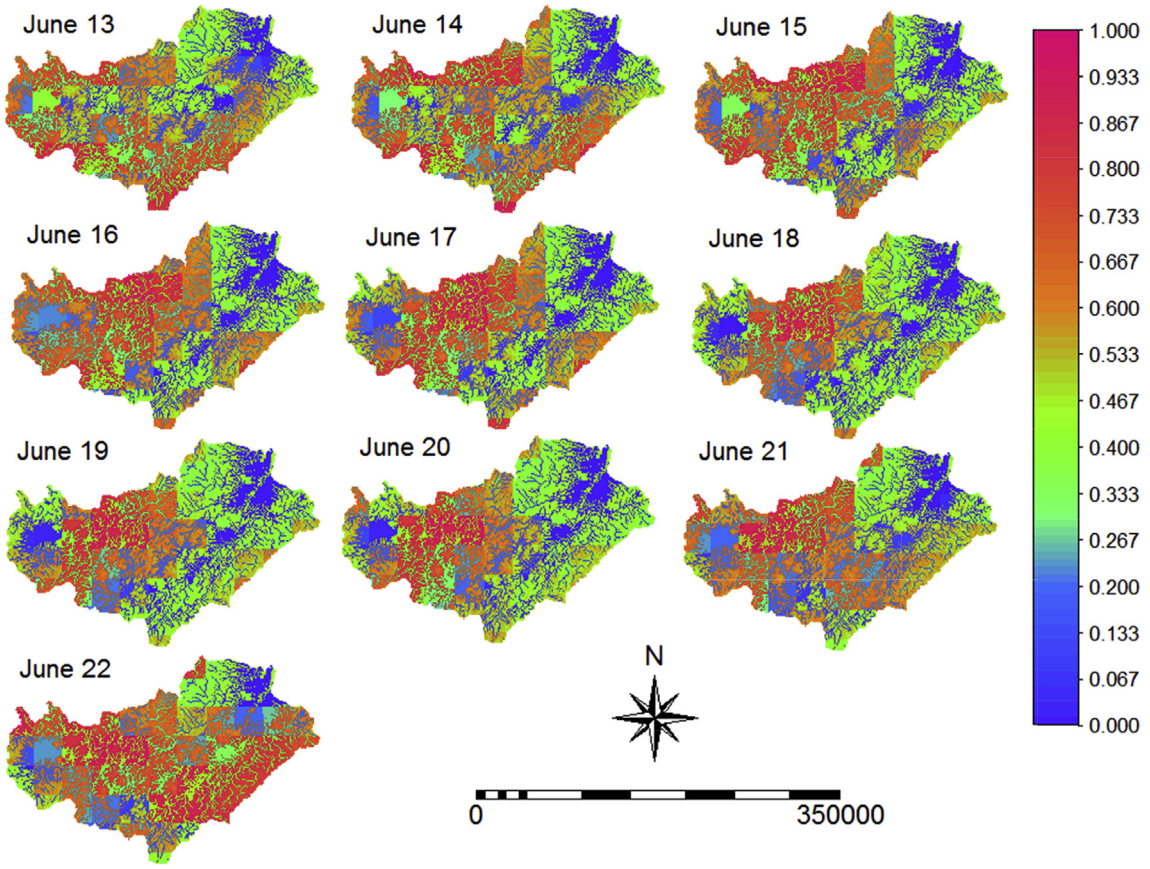

Fig. 9. Flood index distribution for the period June 13–22. The figure illustrates the spatial and temporal variation of the flood index that can be identified with relatively high (pink-red color) and low (green-blue color) value associated with potential and low runoff contributing area respectively. (For interpretation of the references to color in this figure legend, the reader is referred to the web version of this article.).

to calibration parameters were made to improve the match between the observed discharges and simulated counterparts. Prior to calibration, the model was initialized by applying a warm-up period of two year (2005 and 2006).

Calibration was performed for the years 2007 and 2008, whereas 2009 was used for validation. Fig. 6 shows results of calibration and validation. In the year 2008 the simulated highest peak flow (encircled green) is higher than the observed peak flow, whereas in the 2009 simulated peak flow is lower than the observed. For the calibration period in 2007 the first peak in the observed hydrograph is not well simulated. Table 5 shows the calibrated parameter values with the model performance indicators RMSE, NSE and RV_e.

4.2. Analysis of SPI and TWI

For the analysis on SPI and TWI three spatial domains were selected that cover a number of pixels of the CMORPH product with pixel resolution 0.25° by 0.25°. Analysis serves to identify anomalies of rainfall distribution over space of daily SPI of the wet season (June–August) that shows wet pixels (Fig. 7). Fig. 7 show the location of the three spatial domains which mark the upstream areas for identified flood prone areas in the basin. The selections of the sites were done based on areas which may cause flooding in the flood prone areas. Fig. 8 shows time series of daily SPI for the wet season (June–August). The SPI graphs show high SPI values (>1) from June 13–20 and from July 27 – August 04 which indicate wet field conditions. For both periods, the high rainfall may cause flooding in the flood prone areas. According to the information from Ethiopian MoWE (Guinand, 1999; NASA Earth Observatory, 2003; Hydrology department, personal communication) floods in the flood prone areas occur most of the time in the beginning of August (~1st to 8th), during third decade of August (~20th to 27th) and in the beginning of September (~1st to 5th). The incidence of floods during August (~1st to 8th) coincides with the time instant the peak flow in the river channel is predicted. Therefore, high SPI values at pixels in the possible source areas during the second window of time f can be attributed to the occurrence of the floods during the beginning of August. It is noted that results require additional validation by local scale flood modelling that has been ignored in this study. The flood index analysis illustrated the spatial distribution of runoff source areas for floods in the flood prone areas (Figs. 9 and 10).

As shown in Figs. 9 and 10, the spatial and temporal variation of the flood index in the two time windows indicate that pixels can be identified with relatively high value (pink-red colours) and pixels with relatively low values (in green-blue). Pixels with high index values are considered source areas for flooding according to the flood index. In other words, if above average rainfall occurs at such a pixel there is high probability that the areas will be flooded. The maps in Figs. 9 and 10 do not only show the locations of above average rainfall areas but also indicates the changing pattern of above average rainfall in the catchment during the period. To exactly predict the lead time of a flooding event one should further investigate aspects of flood routing from those source areas to the flood prone areas. The above findings indicate that runoff source areas can be well identified when space borne data on rainfall is used and combined with space borne topographic data. As such the flood index is effective as it links time varying rainfall patterns and topographic wetness characteristics which by itself indicate

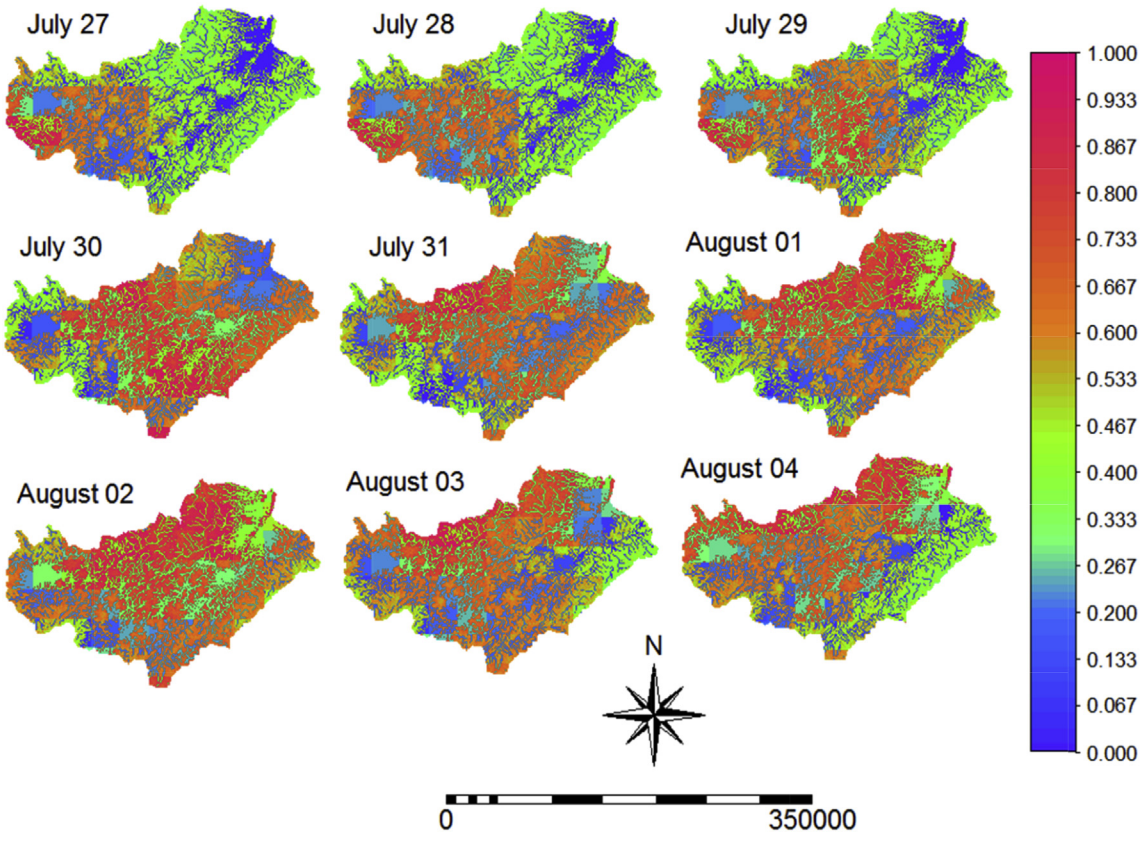

Fig. 10. Flood index distribution for the period July 27 – August. The figure illustrates the spatial and temporal variation of the flood index that can be identified with relatively high (pink-red color) and low (green-blue color) value associated with potential and low runoff contributing area respectively. (For interpretation of the references to color in this figure legend, the reader is referred to the web version of this article.).

potential source areas. By means of a model, runoff from these areas can be simulated to predict high flows. The study also revealed that for each flood prone area the respective locations with above average rainfall can be used as an input for flood index mapping. The latter is of high for NMA since forecasted s above average rainfall could serve for early warning purposes to the communities living in flood prone areas.

5. Conclusions

This study shows effectiveness of spatially distributed remote sensing products for flood early warning. Combining a CMORPH based Standard Precipitation index (SPI) and a SRTM based topographic wetness Index (TWI), this resulted in a Flood index to serve flood early warning. Pixels with high index values are considered source areas for flooding and indicate that above average rainfall at those pixels will cause flood inundation at downstream locations along the river system. Results from integrated runoff and streamflow modelling show that runoff from pixels with high flood index value can be well related to high water events at flood prone areas. For Awash basin, SPI analysis helped to reveal periods over which peak discharges are generated (June 13–20 and July 27 – August 04). Moreover, the flood index that combines SPI and TWI illustrated the spatial distribution of possible runoff source areas with large contributions to flood volumes. Therefore, flood early warning for the ungauged upper and middle Awash River basin can be effective by applying remote sensing based hydrological modelling. Future works should explore the possibility to use runoff models to predict the lead time of the flood event by further investigating flood routing from source areas to the flood prone areas.

Acknowledgment

The authors wish to thank Netherlands Fellowship Program (NFP) who sponsored this research.

References

Abraha, A.A., 2006. Flood Modelling and Forecasting for Awash River Basin in Ethiopia (MSc. thesis). UNESCO-IHE Institute, Delft, Netherlands.
Achamyeleh, K., 2003. The Associated Programme on Flood Management; Integrated Flood Management, Case Study Ethiopia: WMO and GWP. Available at: http://www.apfm.info/pdf/case_studies/cs_ethiopia.pdf. last Retrieved 2015-Aug-25.
Alemayehu, Z., 2007. Modelling of Flood Hazard Management for Forecasting and Emergency Response of 'Koka' Area within Awash River Basin Using Remote Sensing and GIS Method (MSc. thesis). Addis Ababa University, Addis Ababa, Ethiopia.
Alemseged, T.H., Rientjes, T.H.M., 2015. Evaluation of regional climate model simulations of rainfall over the Upper Blue Nile basin. Atmos. Res 161–162, 57–64.
Allen, R.G., Pereira, L.S., Raes, D., Smith, M., 1998. Crop Evapotranspiration – Guidlines for Computing Crop Water Requiremnts – FAO. Irrigation and Drainage Paper 56, FAO Rome.
Allen, R.G., Pruitt, W.O., Raes, D., Smith, M., Pereira, L.S., 2005. Estimating evaporation from bare soil and the crop coefficient for the initial period using common soils information. J. Irrig. Drain. Eng. Asce 131 (1), 14–23.
Beven, K.J., 2012. Rainfall-runoff Modelling: the Primer. John Wiley & Sons, West Sussex. Online ISBN: 9781119951001. DOI: 10.1002/9781119951001.
Beven, K.J., Kirkby, M.J., 1979. A physically based, variable contributing area model of basin hydrology. Hydrol. Sci. Bull. 24, 43–69.
Billa, L., Mansor, S., Mahmud, A.R., Ghazali, A.H., 2006. Modelling rainfall intensity FROM NOAA AVHRR data for operational flood forecasting in Malaysia. Int. J. Remote Sens. 27, 5225–5234.
Budhakooncharoen, S., 2004. Rainfall estimate for flood management using meteorological data from satellite imagery. In: 9th Biennial International Conference on Engineering, Construction and Operations in Challenging Environment, League City Houston, USA.
Burger, G., Reusser, D., Kneis, D., 2009. Early flood warnings from empirical (expanded) downscaling of the full ECMWF ensemble prediction system. Water Resour. Res. 45 (10).
Chen, J.M., Black, T.A., 1992. Defining leaf area index for non-flat leaves. Plant Cell Environ. 15, 421–429.
Dankers, R., Christensen, O.B., Feyen, L., Kalas, M., De Roo, A., 2007. Evaluation of very high-resolution climate model data for simulating flood hazards in The Upper Danube Basin. J. Hydrol. 347, 319–331.
De Roo, A.P.J., Wesseling, C.G., Van Deursen, W.P.A., 2000. Physically based river basin modelling within a GIS: the LISFLOOD model. Hydrol. Process. 14, 1981–1992.
De Roo, A., Schmuck, G., Perdigao, V., Thielen, J., 2003. The influence of historic land use changes and future planned land use scenarios on floods in the oder catchment. Phys. Chem. Earth Parts A/B/C 28, 1291–1300.
Dinku, T., Ceccato, P., Grover-Kopec, E., Lemma, M., Connor, S.J., Ropelewski, C.F., 2007. Validation of satellite rainfall products over East Africa's complex topography. Int. J. of Remote Sens 28, 1503–1526.
ESIG-ALERT, 2004. Early warning systems and sustainable development. In: Early Warning Systems Do's and Don'ts Conference (2003-oct-20–23). Available at: http://www.isse.ucar.edu/alerts/alert6.html. last retrieved 2015-Sept-02.
FEWS NET, 2011. Famine Early Warning System Network, Global Potential Evapotranspiration (PET). Available at: http://earlywarning.usgs.gov/fews/global/web/readme.php?symbol=pt (accessed 30.11.14.).
Feyen, L., Vrugt, J.A., Nualláin, B.Ó., van der Knijff, J., De Roo, A., 2007. Parameter optimisation and uncertainty assessment for large-scale streamflow simulation with the LISFLOOD model. J. Hydrol. 332, 276–289.
Guinand, Y., 1999. UNDP-EUE: Afar Region – Awash River Floods, 09/99. UNDP Emergencies Unit of Ethiopia. Available at: http://www.africa.upenn.edu/Hornet/afar0999.html. last retrieved 2014-Aug-15.
Habib, E., Haile, A.T., Sazib, N., Zhang, Yu., Rientjes, T.H.M., 2014. Effect of bias correction of satellite – rainfall estimates on runoff simulations at the source of the upper Blue Nile. Remote Sens. 6 (7), 6688–6708 open access.
Haile, A.T., Habib, E., Rientjes, T.H.M., 2013. Evaluation of the climate prediction center CPC morphing technique CMORPH rainfall product on hourly time scales over the source of the Blue Nile river. Hydrol. Process. 27 (12), 1829–1839.
Halcrow, 2006. Awash River Basin Flood Control and Watershed Management Study Project. Halcrow and MoWE, Addis Ababa, Ethiopia.
Joyce, R.J., Janowiak, J.E., Arkin, P.A., Xie, P., 2004. CMORPH: a method that produces global precipitation estimates from passive microwave and infrared data at high spatial and temporal resolution. J. Hydrometeorol. 5 (3), 487–503.
Jarvis, A., Reuter, H.I., Nelson, A., Guevara, E., 2008. Hole-filled Seamless SRTM Data V4. International Centre for Tropical Agriculture (CIAT) last retrieved 2015-Aug-20 at. http://srtm.csi.cgiar.org.
Laguardia, G., Niemeyer, S., 2008. On the comparison between the LISFLOOD modelled and the ERS/SCAT derived soil moisture estimates. Hydrol. Earth Syst. Sci. 12, 1339–1351.
Liu, J., Duan, Z., Jiang, J., Zhu, A., 2015. Evaluation of Three Satellite Precipitation Products TRMM 3B42, CMORPH, and PERSIANN over a Subtropical Watershed in China. Adv. Meteorol. Article ID 151239. DOI: 10.1155/2015/151239.
Maathuis, B.H.P., Mannaerts, C.M., Lemmens, R.L.G., Schouwenburg, M.L., Retsios, V., 2014. GEONETCast Toolbox. Installation, Configuration and User Guide of the GEONETCast-toolbox Plug-in for ILWIS 3.7. Version1.6. Available at: http://52north.org/downloads/earth-observation.
McKee, T.B., Doesken, N.J., Kleist, J., Amer Meteorol, S.O.C., 1993. The relationship of drought frequency and duration to time scales. In: The 8th Conference on Applied Climatology. Available at: http://ccc.atmos.colostate.edu/relationshipofdroughtfrequency.pdf. last retrieved 2015-Aug-10.
Moore, I.D., Norton, T.W., Williams, J.E., 1993. Modelling environmental heterogeneity in forested landscapes. J. Hydrol. 150, 717–747.
MoWE, 2011. Nature and Features of the Ethiopian River Basins. Ministry of Water and Energy. Available at: http://www.mowr.gov.et/index.php?pagenum=3.1&pagehgt=5500px. last retrieved 2014-Aug-15.
NASA Earth Observatory, 2003. Flooding along the Awash River in Ethiopia.. Available at: http://earthobservatory.nasa.gov/NaturalHazards/view.php?id=12065. last retrieved 2015-Aug-16.
Robson, A., Beven, K., Neal, C., 1992. Towards identifying sources of subsurface flow – a comparison of components identified by a physically based runoff model and those determined by chemical mixing techniques. Hydrol. Process. 6, 199–214.
Roujean, J.L., Lacaze, R., 2002. Global mapping of vegetation parameters from POLDER multiangular measurements for studies of surface-atmosphere interactions: a pragmatic method and its validation. J. Geophys. Res. 107D, 10129–10145.
Salamon, P., Feyen, L., 2009. Assessing parameter, precipitation, and predictive uncertainty in a distributed hydrological model using sequential data assimilation with the particle filter. J. Hydrol. 376, 428–442.
Seibert, J., McGlynn, B., 2007. A new triangular multiple flow direction algorithm for computing upslope areas from gridded digital elevation models. Water Resour. Res. 43, W04501. http://dx.doi.org/10.1029/2006WR005128.
Seiler, R.A., Hayes, M., Bressan, L., 2002. Using the standardized precipitation index for flood risk monitoring. Int. J. Climatol. 22, 1365–1376.
Taddese, G., Peden, D., Sonder, K., 2006. The Water of the Awash River Basin a Future Challenge to Ethiopia. International Livestock Research Institute (ILRI), Addis Ababa, Ethiopia. Available at: http://www.iwmi.cgiar.org/assessment/files/pdf/publications/WorkingPapers/WaterofAwasBasin.pdf. last retrieved 2015-Oct-10.
Thielen, J., Bartholmes, J., Ramos, M., De Roo, A., 2009. The European flood alert system – part 1: concept and development. Hydrol. Earth Syst. Sci. 13, 125–140.
Thiemig, V., Pappenberger, F., Thielen, J., Gadain, H., De Roo, A., Bodis, K., Muthusi, F., 2010. Ensemble flood forecasting in Africa: a feasibility study in The Juba-

Shabelle River Basin. Atmos. Sci. Lett. 11, 123–131.
Thiemig, V., De Roo, A., Gadain, H., 2011. Current status on flood forecasting and early warning in Africa. Int. J. River Basin Manag. 9, 63–78.
UNISDR, 2009. UNISDR Terminology on Disaster and Risk Reduction. UN International Strategy for Disaster Reduction, Geneva, Switzerland. Available at: http://www.unisdr.org/files/7817_UNISDRTerminologyEnglish.pdf. last retrieved 2015-Oct-12.
Van der Knijff, J., De Roo, A., 2008. LISFLOOD Distributed Water Balance and Flood Simulation Model. Revised User Manual. ISSN: 1018-5593. Joint Research Centre, European Commision, Luxembourg, p. 109.
Western, A.W., Grayson, R.B., Blöschl, G., Willgoose, G.R., McMahon, T.A., 1999. Observed spatial organization of soil moisture and its relation to terrain indices. Water Resour. Res. 35, 797–810.
WMO, 2009. In: Integrated Flood Management; Concept Paper. World Meteorological Organization, Geneva, Switzerland. Available at: Retrieved from URL. http://www.apfm.info/pdf/concept_paper_e.pdf. last retrieved 2015-Agust-26.
World Bank, 2007. Ethiopia – Eastern Nile Flood Preparedness and Early Warning (Phase 1) Project. Washington DC, USA.